Enhancement of Superelasticity in Cu-Al-Mn-Ni Shape-Memory Alloys by Texture Control

Y. SUTOU, T. OMORI, R. KAINUMA, N. ONO, and K. ISHIDA

A significant improvement in the degree of superelasticity in Cu-Al-Mn ductile polycrystalline alloys has been achieved through the addition of Ni and control of the recrystallization texture by thermomechanical processing, which contain the annealing in the fcc (α) + bcc (β) two-phase region, followed by heavy cold reductions of over 60 pct. The addition of Ni to the Cu-Al-Mn alloys shows a drastic effect on the formation of the strong $\{112\}\langle 110\rangle$ recrystallization texture. Superelastic strains on the order of 7 pct, 3 times larger than those in other Cu-based shape-memory alloys (SMAs), have been realized in the textured Cu-Al-Mn-Ni alloys. The superelastic strains obtainable in the textured Cu-based SMAs are on a par with those attainable in Ni-Ti–based alloys.

I. INTRODUCTION

Cu-BASED shape-memory alloys (SMAs), such as Cu-Zn-Al and Cu-Al-Ni, are commercially attractive systems for the practical exploitation of the shape-memory effect (SME) and superelasticity (SE) and stand next in line to Ni-Ti as suitable alloys for SM applications, because of their low cost and their advantages with regard to electrical and thermal conductivities.[1,2] However, Cu-based SMAs with a polycrystalline structure are too brittle to be sufficiently cold worked and possess a low degree of shape recovery in the SME and SE.[1,2] The brittleness of the β-polycrystalline Cu-based alloys arises from the high degree of order in the parent β phase with a B2, DO_3, or $L2_1$ structure and the unusually high elastic anisotropy ratios of $A = 2c_{44}/(c_{11} - c_{12}) = 13$ and $A = 15$ for Cu-Al-Ni and Cu-Zn-Al SM alloys in the parent β phase, respectively,[1] where c_{44}, c_{11}, and c_{12} are the elastic stiffness. The coarse grain structure associated with the β phase in these alloys exacerbates this proneness to brittleness even further. Many attempts to improve the ductility by grain refining have been made, but only limited success has been reported.[1,3]

Figure 1 shows the vertical section of the phase diagram of the Cu-Al-10 at. pct Mn system,[4] where the single-phase β region is seen to be broadened by the addition of Mn. It can also be seen that the transition temperatures associated with two types of order-disorder transitions, β (A2) $\rightarrow$ β_2 (B2) and $\beta_2 \rightarrow \beta_1$ ($L2_1$), decrease with decreasing Al content. Recently, Kainuma *et al.* have found that the Cu-Al-Mn–based alloys with an Al content below 18 at. pct (low degree of order) show excellent cold workability, good ductility, and also exhibit the SME and SE based on cubic β_1 ($L2_1$) to monoclinic β_1' (18R) martensitic transformation.[5,6] However, the SE strain is still limited to the region below 2 pct in these alloys and is not yet sufficient for practical applications in many fields. Very recently, the present authors have investigated the effect of alloying elements such as Ni, Co, *etc.* on the SME and SE of these alloys[7] and found that the Ni addition considerably enhances the ductility of the specimens after annealing at temperatures between 773 and 1073 K,[8] although the SME and SE properties are not significantly improved.

Commercial Ni-Ti–based SMAs are prepared by conventional casting techniques followed by thermomechanical processing (TMP), which is a combination of cold working or hot rolling and low-temperature annealing at 673 to 773 K that yields a favorably textured Ni-Ti polycrystalline alloy.[9–12] Texture is one of the reasons why the strains recoverable in Ni-Ti alloys are so much larger than those in Cu-based SMAs.[13] Although it has been predicted theoretically that the formation of a particular texture should improve the SM properties in Cu-based alloys,[13,14] the usual fabrication methods have not been successful in inducing a favorable texture with resultant enhancement of the SM properties. This is mainly due to the relatively low cold workability and the requirement for high-temperature annealing over 873 K. Splat quenching has been the only method, so far, to result in a favorable texture in the columnar grains of the splat with good SM and SE properties.[9,15] Since the recently identified ductile Cu-Al-Mn–based alloys exhibit excellent cold workability, it was expected that a favorable texture could be induced by a proper TMP treatment in order to improve the SM and SE properties in these alloys.

In the present study, the effects of TMP and an Ni addition on the SE in the Cu-Al-Mn alloys were investigated, focusing on the texture development.

II. EXPERIMENTAL PROCEDURES

Three kinds of alloys, $Cu_{71.5}Al_{17}Mn_{11.5}$ (designated as 0Ni), $(Cu_{73}\text{-}Al_{17}\text{-}Mn_{10})_{98}\text{-}Ni_2$ (designated as 2Ni), and $(Cu_{73.5}\text{-}Al_{17}\text{-}Mn_{9.5})_{97}\text{-}Ni_3$ (designated as 3Ni), with an expected martensitic transformation starting temperature (M_s) in the interval of 215 to 240 K, were prepared by induction melting in an argon atmosphere.[7] The scheme for preparation of sheet specimens of these alloys was as follows: (1) hot rolling at 1073 K from a 20-mm-diameter ingot to a thickness of 2 mm, (2) annealing in the α (fcc) + β (bcc) region at 873 K basically for 600 seconds, (3) cold rolling

Y. SUTOU, JSPS Researcher, T. OMORI, Graduate Student, R. KAINUMA, Associate Professor, and K. ISHIDA, Professor, are with the Department of Materials and Science, Graduate School of Engineering, Tohoku University, Sendai 980-8579, Japan. Contact e-mail: kainuma@material.tohoku.ac.jp N. ONO, Professor, is with the Department of Mechanical Systems on Information Technology, Hachinohe Institute of Technology, Hachinohe 031-8501, Japan.

Manuscript submitted October 5, 2001.

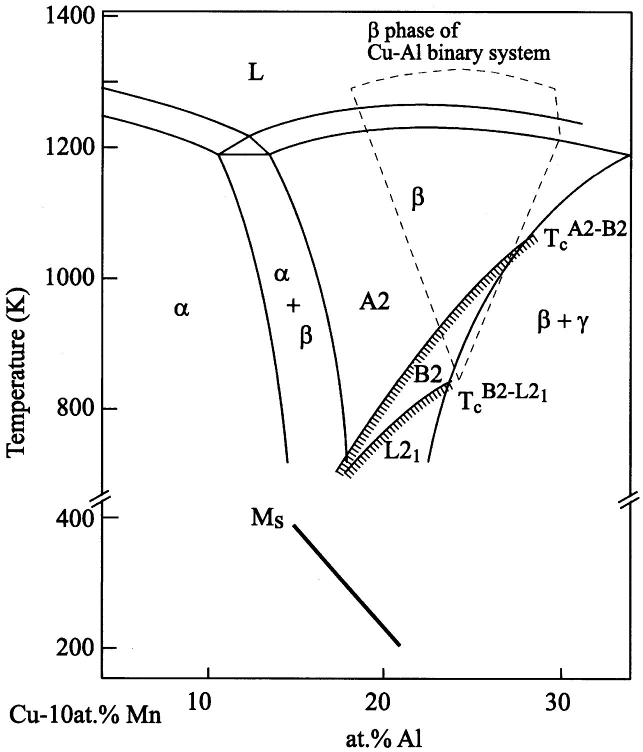

Fig. 1—Vertical section diagram of the Cu-Al-10 at. pct Mn system with A2/B2 and B2/$L2_1$ order-disorder transition boundaries[4] and martensitic transformation temperatures.[5,6]

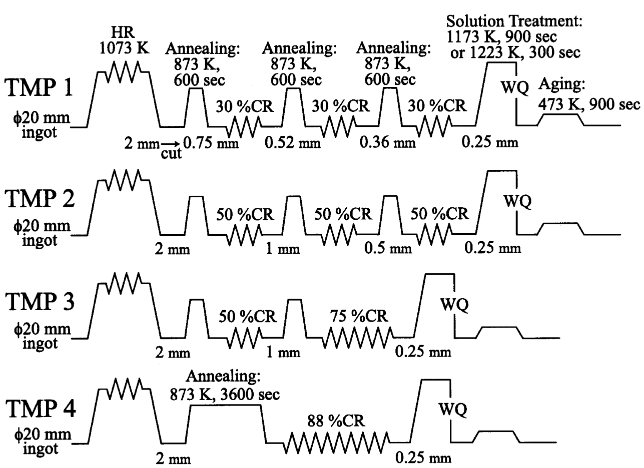

Fig. 2—Schematic illustration of the thermomechanical processes employed. HR, CR, and WQ indicate "hot rolling," "cold rolling," and "water quenching," respectively. The annealing time in the TMP4 was prolonged up to 3600 seconds to obtain enough ductility in the following heavy cold rolling.

down to a thickness corresponding to a reduction ratio between 30 and 88 pct, (4) solution treatment at 1173 K for 900 seconds or at 1223 K for 300 seconds, and (5) quenching in iced water followed by aging at 473 K for 900 seconds to stabilize the martensitic transformation temperatures. A schematic illustration of the thermomechanical processes employed (TMP1 through 4) is shown in Figure 2. The volume fraction of the α phase after the final annealing at 873 K, performed in each TMP treatment, was measured by quantitative metallography. The transformation temperatures M_s and A_f were determined by differential scanning calorimetry at a heating and cooling rate of 0.17 K/s. Table I shows the α-phase volume fraction after the final annealing at 873 K, the grain size (d), the relative grain size (d/t, t being the specimen thickness), and transformation temperatures after the various TMPs treatments, as shown in Figure 2. The recrystallization texture determinations were carried out by orientation-imaging microscopy and electron backscattered Kikuchi diffraction (EBSD).[16] The SE was examined by cyclic load in tensile testing using an Instron machine at a strain rate of 0.83×10^{-2} mm/s at a temperature 30 K higher than the reverse-transformation finishing temperature (A_f). The size of the tensile specimen in the gage-length portion was $20 \times 4.5 \times 0.25$ mm^3 (length $\times$ width $\times$ thickness), and the SE strains were measured using an extensometer.

The lattice parameters of the parent and the martensite phases used for the calculations of the orientation dependence of the transformation strain were determined by X-ray diffraction at room temperature. Moreover, a single crystal of the Cu_{73}-Al_{17}-Mn_{10} β phase, with a size of $30 \times 3 \times 0.2$ mm^3 (length $\times$ width $\times$ thickness), was prepared by the secondary recrystallization method. The transformation strain in a single crystal was measured by tensile testing at a strain rate of 0.83×10^{-2} mm/s at $A_f + 30$ K.

III. RESULTS AND DISCUSSION

A. *Recrystallization Texture*

The normal direction (ND), rolling direction (RD), and transverse direction (TD) of the sheet are defined in Figure 3(a). Figures 3(c) through (e) are quasi-colored orientation maps obtained by the EBSD technique in the ND, RD, and TD, respectively, taken from the 3Ni alloy specimens in the quenched condition after the TMP4 treatment. The color of each grain in the mapped microstructures in Figures 3(c) through (e) indicates the crystal direction parallel to the ND, RD, and TD, respectively, displayed with the same color as that in the reference-unit stereographic triangle (Figure 3(b)). From Figures 3(c) through (e), it is seen that the texture densities in the ND, RD, and TD directions have their largest value around the [112], [101], and [111] directions, respectively. In addition, it is also found by EBSD analysis that about 30 pct of the grain boundaries are small-angle boundaries misorientated within 15 deg. Figure 4 shows the (100), (110), and (111) pole figures of the aforementioned specimens of the 3Ni alloy. It can be seen that the $\{112\}\langle 110\rangle$ orientations are consistent with the highest-intensity regions of the pole figures. The other orientations, such as $\{111\}\langle 112\rangle$ and $\{001\}\langle 110\rangle$, can be considered as minor orientations. Such a recrystallization texture was detected in all the specimens examined in the present study. Figures 5(a) through (c) are plots of the texture intensity as a function of the final reduction level attained at the end of every TMP treatment. They show the change in texture intensity in the [112], [101], and [111] components for the ND, RD, and TD axes, respectively, for every alloy that was cold rolled down to various degrees of reduction, as per every TMP treatment, and recrystallized at 1173 K for 900 seconds after each TMP treatment. It is seen that the [112], [101], and [111] intensities along the ND, RD, and TD axes are very low and remain almost the same with increasing final rolling

Table I. Volume Fraction of the α Phase after Final Annealing at 873 K, M_s, and A_f Temperatures, Average Grain Size (d) and Relative Grain Size (d/t) (t: specimen thickness) of β Phase after Various TMPs

Alloy Designation	Alloy Composition (At. Pct)	Volume Fraction of α Phase after Final Annealing at 873 K (Pct)	Thermo-mechanical Process	M_s (K)	A_f (K)	d (μm)	d/t
0Ni	$Cu_{71.5}$-Al_{17}-$Mn_{11.5}$	42	TMP 1	215	240	405	1.6
		42	TMP 2	221	239	302	1.2
2Ni	$(Cu_{73}$-Al_{17}-$Mn_{10})_{98}$-Ni_2	75	TMP 1	231	242	421	1.7
		75	TMP 2	227	243	353	1.4
		75	TMP 3	223	239	368	1.5
3Ni	$(Cu_{73.5}$-Al_{17}-$Mn_{9.5})_{97}$-Ni_3	>90	TMP 2	235	249	285	1.1
		>90	TMP 3	239	254	277	1.1
		>90	TMP 4	240	253	227	0.9

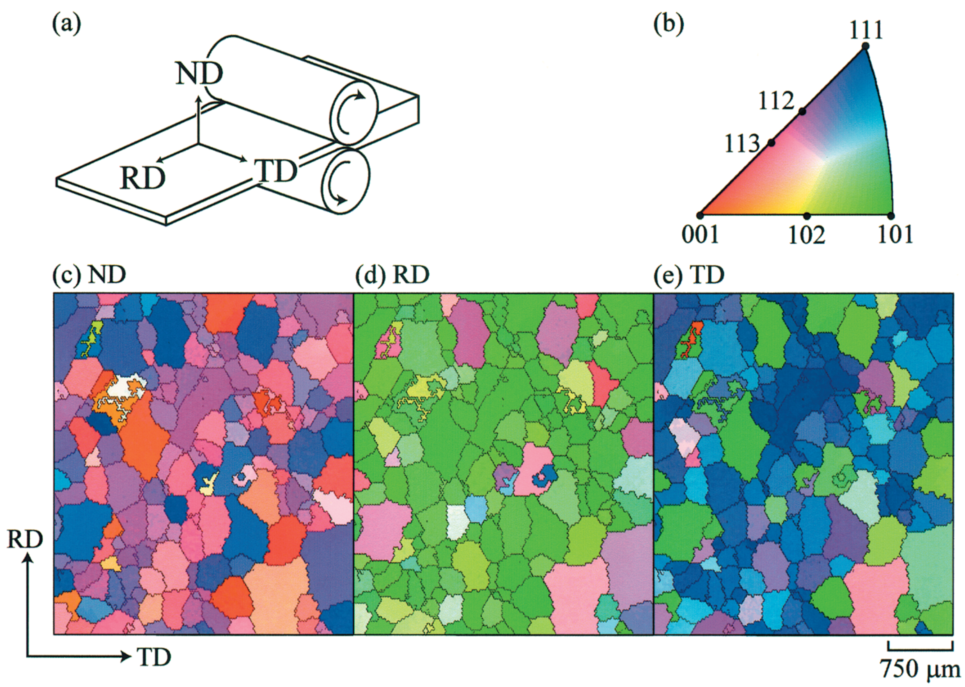

Fig. 3—(a) Sheet rolling—reference directions, (b) the reference unit stereographic triangle, (c) through (e) the quasi-colored orientation mapping microstructures taken from the specimens of 3Ni alloy cold rolled by 88 pct and solution treated at 1223 K for 300 seconds (TMP4), which were obtained by EBSD.

reduction in the Cu-Al-Mn ternary alloy, while each orientation intensity for the quaternary alloys containing Ni is much higher than that of the ternary alloy and increases with increasing final rolling reduction. It is apparent that the [112], [101], and [111] orientations in the ND, RD, and TD, respectively, are greatly enhanced with increasing rolling reduction and recrystallization in the 3Ni alloy.

The reasons why the addition of Ni enhances the texture in the Cu-Al-Mn alloy are not clear at present, but it may be related to the fact that such an addition results in an increment of volume fraction of the α (fcc) phase at the annealing temperature of 873 K.[17] Figures 6(a) through (c) show the ($\alpha + \beta$) two-phase microstructure obtained by optical microscopy after the final annealing at 873 K performed in TMP2 treatment, and the volume fractions of the α phase in those microstructures are listed in Table I. It is seen that the volume fraction of the α phase increases with increasing Ni content and that the microstructure of the 3Ni specimen, with an α volume fraction over 90 pct, is very fine compared with the ternary alloy. Furthermore, it should be noted that the cold rolling of the β single phase after quenching does not promote the formation of texture.[8] These facts suggest that the volume fraction of the α phase after annealing is an important factor in texture control.

B. *Prediction of the Transformation Strains in Cu-Al-Mn Alloys*

For the present Cu-Al-Mn–based alloys, the 18R β_1' martensite phase is formed from the β_1 ($L2_1$) parent phase by the thermal and stress-induced martensitic transformations, which cause the SME and SE. The magnitude of the SM and SE strains of a single crystal as a function of the crystal directions and the loading direction can be evaluated on the basis of the phenomenological theory of martensitic transformations.[18,19] In many SMAs, the orientation dependence of the transformation strain (TS) has been calculated by using the shape strain or the lattice-deformation matrix.[20,21] In the case of using shape strain, the TS in single crystals

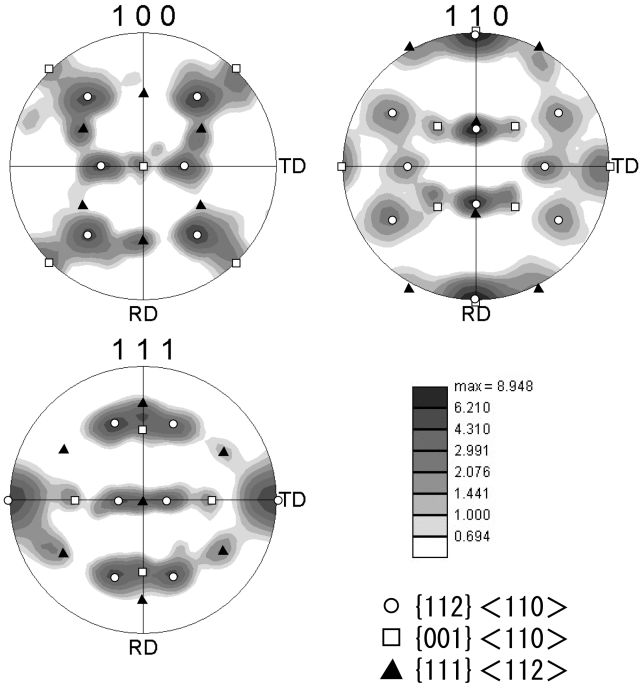

Fig. 4—(100), (110), and (111) pole figures of the specimens of 3Ni alloy cold rolled by 88 pct and solution treated at 1223 K for 300 seconds (TMP4).

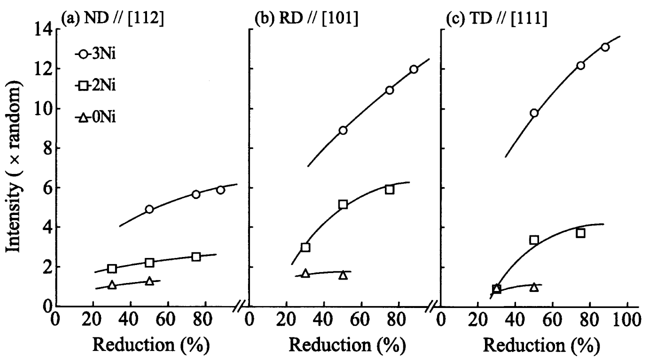

Fig. 5—The plots of texture intensity of [112], [101], and [111] components in (*a*) ND, (*b*) RD, and (*c*) TD, respectively, against the final rolling reduction.

induced by the β_1/β_1' transformation in tension can be expressed as follows:

$$\mathrm{TS} = \sqrt{\eta^2 \cos^2 \chi + 2\eta \cos \lambda \cos \chi + 1} - 1 \qquad [1]$$

where η is the magnitude of shape strain, χ is the angle between the habit-plane normal and the tensile axis, and λ is the angle between the shape-strain direction and the tensile axis. The phenomenological data required for evaluating the orientation dependence of the TS are calculated by lattice parameters which were obtained by X-ray diffraction from the Cu_{73}-Al_{17}-Mn_{10} ternary alloy. The lattice parameters used for the calculations (the habit-plane normal (h), the shape-strain direction (d), and the magnitude of shape strain (η)), calculated by the phenomenological analysis of the β_1/β_1' transformation in the Cu-Al-Mn alloy based on the Wechsler–Lieberman–Read[18] theory, are summarized in Table II.

Figure 7(a) shows the iso-TS contour lines corresponding to the β_1/β_1' transformation in tension of the Cu_{73}-Al_{17}-Mn_{10}

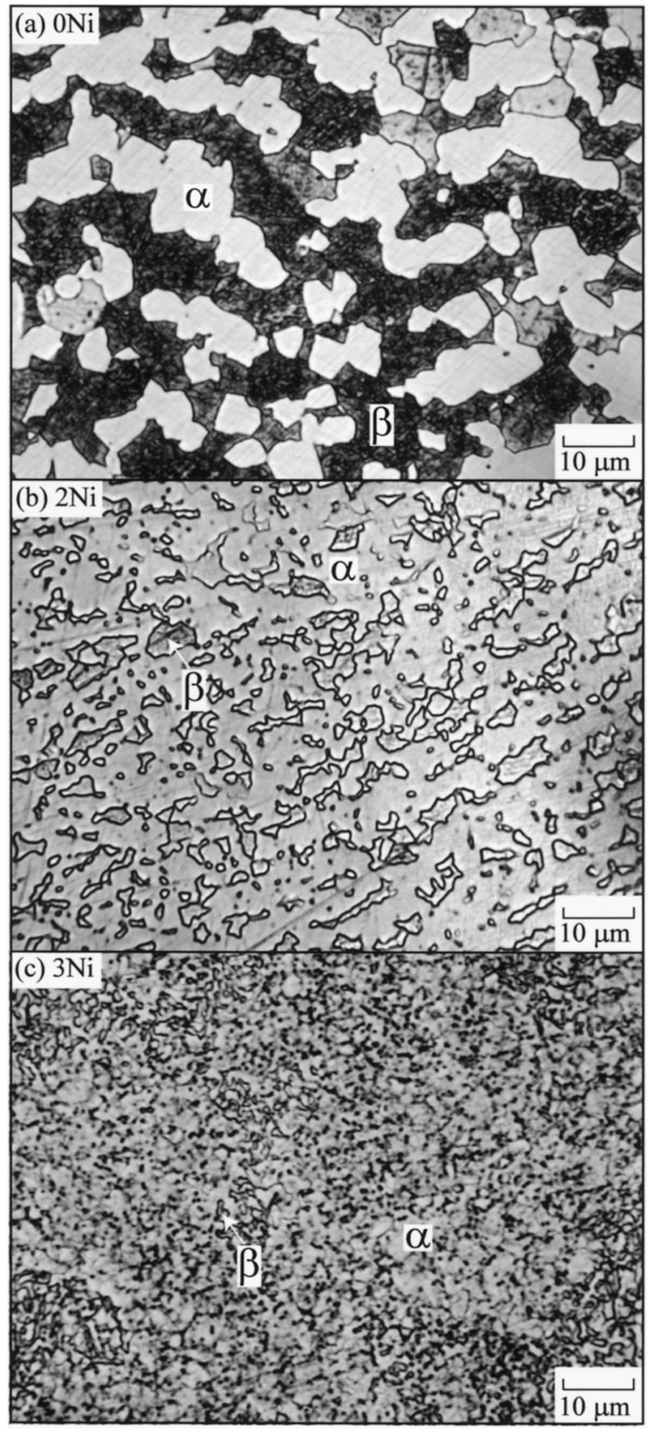

Fig. 6—Optical microstructures after final annealing at 873 K performed in TMP2: (*a*) 0Ni, (*b*) 2Ni, and (*c*) 3Ni.

single crystal, calculated using Eq. [1]. It is deduced from the stereographic triangle of Figure 7(a) that a maximum TS of 10.3 pct occurs in a direction lying between [001] and [102] and that the TS in the [101] and [111] directions is about 7.5 and 2 pct, respectively, similar to the ones calculated for other Cu-based SMAs.[20,21,22] The experimental data of TS in tension, obtained from the Cu_{73}-Al_{17}-Mn_{10} single crystal (present work) and Cu_{70}-Al_{20}-Mn_{10} single crystal (the work of Kato *et al.*[23]), are also shown in Figure

Table II. Lattice Parameters Used for the Phenomenological Analysis, and Quantities from Phenomenological Theory Used for Calculation of Transformation Strain; *h*: Habit Plane Normal, *d*: Shape Strain Direction, and η: Magnitude of Shape Strain

Lattice Parameters				
Parent β_1	Martensite β_1'	h	d	η
$a_0 = 0.5864$ nm	$a = 0.4453$ nm $b = 0.5299$ nm $c = 3.834$ nm $\beta = 89.10°$	$\begin{bmatrix} 0.15547 \\ -0.67679 \\ 0.71957 \end{bmatrix}_{\beta_1}$	$\begin{bmatrix} 0.14049 \\ 0.74663 \\ 0.65024 \end{bmatrix}_{\beta_1}$	0.19953

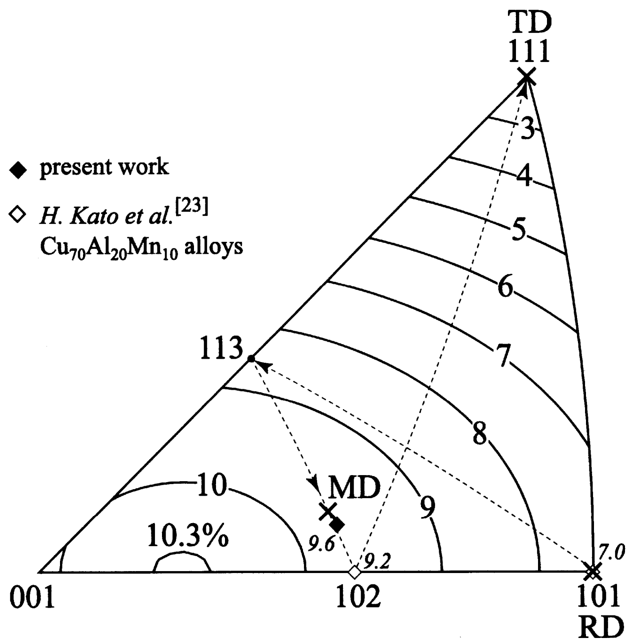

(*a*)

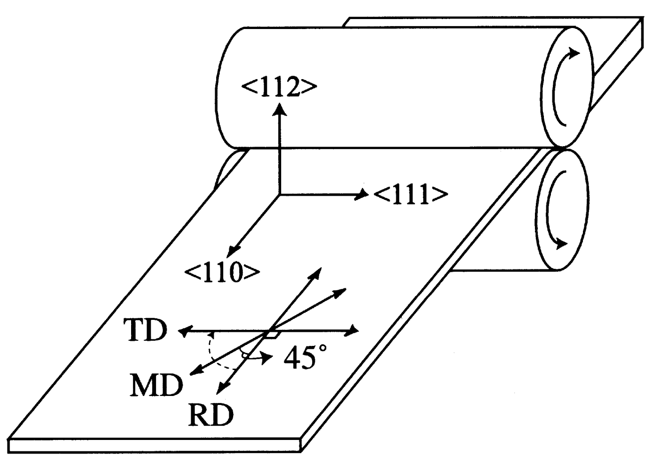

(*b*)

Fig. 7—(*a*) Contour lines of isotransformation strain induced by the β_1/β_1' transformation obtained by the calculation. (*b*) Loading directions in the sheet specimens and the corresponding textures observed in the 3Ni alloy. The rotation of loading direction in the sheet plane from RD to TD *via* MD (b) corresponds to the direction path RD $\rightarrow$ MD $\rightarrow$ TD, as indicated by the broken line in (a).

7(a). There is good agreement between theoretical and experimental findings.

C. *Effect of Texture on the SE Strain of Sheet Specimens*

The effect of texture on the SE strain was investigated by using the 3Ni alloy cold rolled by 88 pct and solution treated at 1223 K for 300 seconds (TMP4), with the strong $\{112\}\langle 110\rangle$ recrystallization texture. In the case of the $\{112\}\langle 110\rangle$ textured sheet, the RD and TD are parallel to $\langle 110\rangle$ and $\langle 111\rangle$, respectively, as illustrated in Figure 7(b). To change the loading direction from the RD to TD in the sheet plane, the loading axis must be rotated from the RD to TD *via* a middle direction (MD), which is at an angle of 45 deg from the RD. This corresponds to the direction path RD $\rightarrow$ MD $\rightarrow$ TD, indicated as the broken line in Figure 7(a). It can be seen that the largest TS is obtained at around the MD, and the SE strain in the MD is expected to be the largest in all tensile directions.

Figures 8(a) through (c) show the stress-strain curves in the cyclic load obtained for the specimens cut along the loading directions RD, MD, and TD in the sheet plane, where these sheet specimens have the value of $d/t = 1.2$. These specimens were loaded in tension up to a strain of $\varepsilon_t^{i(=1)}$ ($\sim$2 pct) at first and then unloaded to a strain of $\varepsilon_r^{i(=1)}$, then were reloaded up to a strain of $\varepsilon_t^{i(=2)}$ ($\sim$4 pct) in the second cycle and then unloaded to $\varepsilon_r^{i(=2)}$ and so forth, where $\varepsilon_t^{\,i}$ is the strain applied to the specimen, $\varepsilon_r^{\,i}$ is the residual strain after removal of the stress, and *i* is the number of cycles, as illustrated in Figure 8(a). It can be seen that the degree of shape recovery is strongly dependent on the loading direction, and the specimen in the MD shows the highest degree of SE, as expected. Figure 9 shows the variation of $\varepsilon_{SE}^{\,i}$ in the specimens with the applied strain $\varepsilon_t^{\,i} - \varepsilon_e^{\,i}$, where $\varepsilon_e^{\,i}$ is the genuine elastic strain, which varies in each textured specimen, and $\varepsilon_{SE}^{\,i}$ is the SE strain, defined by $\varepsilon_{SE}^{\,i} = \varepsilon_t^{\,i} - \varepsilon_e^{\,i} - \varepsilon_r^{\,i}$, as illustrated in Figure 8(a). The $\varepsilon_{SE}^{\,i}$ increases with applied strain in the initial stage and then decreases after reaching the maximum point ($\varepsilon_{SE}^{\mathrm{MAX}}$) in the MD and RD specimens, while the TD specimen fractured before reaching a maximum point. In the present study, the high level of the SE strain ($\varepsilon_{SE}^{\mathrm{MAX}} \approx 7$ pct) was obtained in the MD sheet, where the SE is hardly affected by the cyclic effect. It was actually confirmed that the $\varepsilon_{SE}^{\,1}$ value in the specimen performed up to $\varepsilon_t^{\,1} = 8$ pct by one cycle and the $\varepsilon_{SE}^{\,4}$ value in the specimen performed up to $\varepsilon_t^{\,4} = 8$ pct by four cycles, as shown in Figure 8, are almost equal. On the other hand, the value of the recoverable strain in the Cu-Al-Mn ternary alloys cannot be improved by TMP, even if the loading direction is rotated from the RD to TD *via* the MD, because no strong texture is formed, as shown in Figures 10(a) through (c). It can be concluded from these results that the SE strain is strongly dependent on the texture.

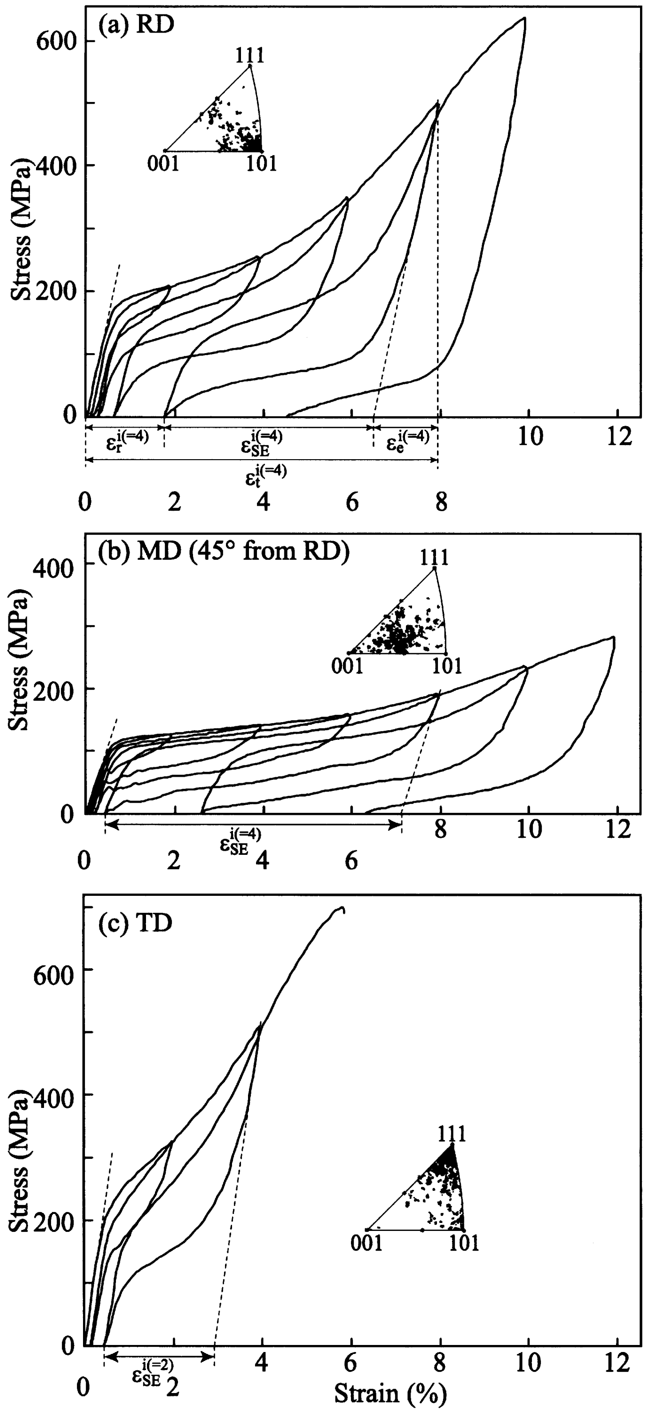

Fig. 8—Cyclic stress-strain curves obtained from specimens at A_f + 30 K cut along the loading direction RD, MD, and TD in (*a*) through (*c*) the 3Ni sheet plane.

In addition, it must be noticed that the $\varepsilon_{SE}{}^{\mathrm{MAX}}$ term defined in this study is not the maximum strain associated with the stress-induced martensitic transformation in a polycrystalline state, because the $\varepsilon_r{}^i$ value at testing temperature includes both the plastic and residual strains due to stabilized martensite (ε_M), which can be removed by heating. Therefore, the value of $\varepsilon_{SE}{}^{\mathrm{MAX}} + \varepsilon_M$ should be compared with the TS of the single crystal predicted in Figure 7(a).

Ono *et al.*[24] have reported on the recovery strain in the polycrystalline SMAs based on the Taylor model. According

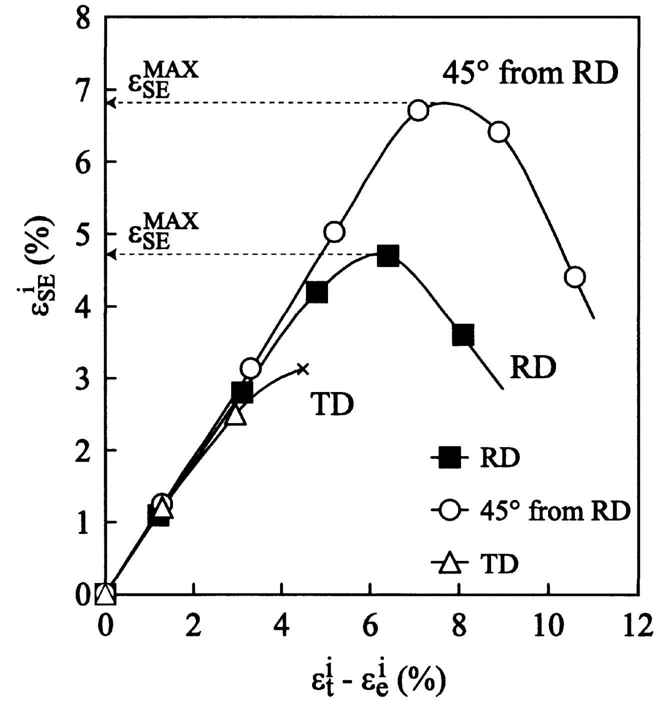

Fig. 9—Plot of the SE strain $\varepsilon_{SE}{}^i$ *vs* the applied strain $\varepsilon_t{}^i - \varepsilon_e{}^i$.

to their calculations on the β_1/β_1' transformation in the Cu-Zn-Al alloy, which is similar to that in the Cu-Al-Mn alloy, the recovery strain in tension at the MD is about 2 pct.[24] The SE strain of 7 pct at the MD obtained in this study, however, is much larger than the calculated one. This is because the results of calculations by Ono *et al.* are available for the case where only the tensile axis shows texture and the other two are randomly distributed such as in fiber-textured SMAs, while the textured sheets obtained in this study show a single-crystal texture.

The present results on the SE strain are in agreement with the predictions by Shu and Bhattacharya,[13] who showed that the largest value would be obtained at an angle of 45 deg from the RD in the polycrystalline Cu-based alloys with a $\{001\}\langle 110\rangle - \{112\}\langle 110\rangle$ texture, which is similar to the present Cu-Al-Mn-Ni–textured alloys. However, the predicted recoverable strain at an angle of 45 deg from the RD of the Cu-Zn-Al alloys is only about 3.5 pct, which is lower than the SE strain observed in this study. This difference is probably related to the grain-size effect. It is known that recoverable strain depends on the relative grain size and increases with increasing d/t values, *i.e.*, the recoverable strain increases with decreasing grain constraint.[25] The degree of grain constraint in the tensile-tested 3Ni specimens with $d/t = 1.2$ may be small, since most of the β grains extend through the specimen thickness. Shu and Bhattacharya[13] have also reported that in the case of specimens with columnar grains (*i.e.*, grains which extend through the thickness) such as thin films, large recovery strain is obtained in some tensile directions. The details of the effect of grain size on the SM properties will be reported before long.[26]

Table III shows a comparison of the cold workability and SM properties in the three systems, Cu-Al-Mn-Ni, Cu-Zn-Al, and Ni-Ti.[2,27] The SE strain of about 7 pct obtained in the Cu-Al-Mn-Ni–textured alloy is over 3 times greater than the maximum value obtainable in any of the polycrystalline

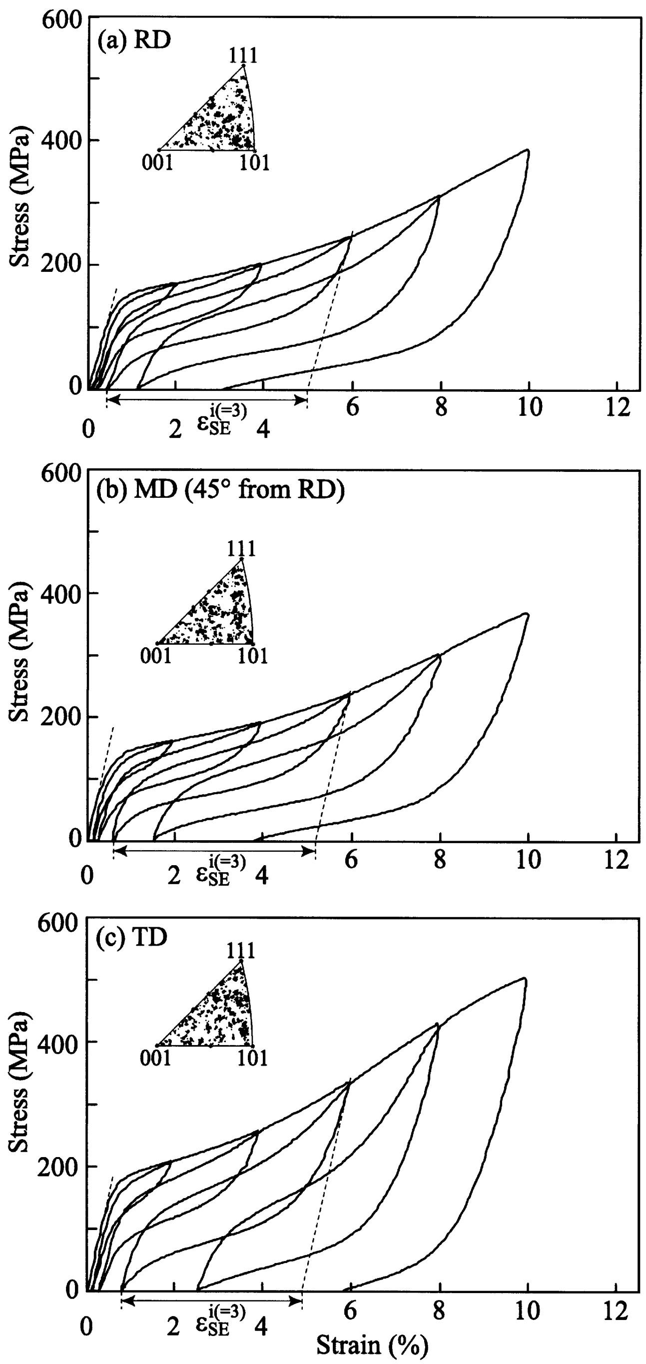

Fig. 10—Cyclic stress-strain curves obtained from specimens at $A_f + 30$ K cut along the loading direction RD, MD, and TD in (*a*) through (*c*) the 0Ni sheet plane.

Table III. Comparison of Cold Workability and SE in the Polycrystalline Cu-Al-Mn-Ni, Cu-Zn-Al, and Ni-Ti Alloys[2,27]

	Cold Workability	ε_{SE}^{MAX}
Cu-Al-Mn-Ni	~80 pct	7 pct
Cu-Zn-Al	<30 pct	2 pct
Ni-Ti	~30 pct	8 pct

Cu-based SM alloys previously reported and is comparable to that obtained in the Ni-Ti alloys. Since the Cu-Al-Mn-Ni SMAs exhibit excellent cold workability, they can be easily fabricated not only as sheets, but also as foil, fine wire, and tubes. This new system of Cu-Al-Mn-Ni SMAs has high potential for practical applications as SE component materials in electrical and medical devices, micromachines, and energy-storage technology applications.

IV. CONCLUSIONS

Texture control by TMP treatments was investigated in Cu-Al-Mn–based alloys with enhanced cold workability, with a view to improving their SM and SE properties. The results obtained are as follows.

1. The {112}⟨110⟩ recrystallization texture was developed and enhanced in the Cu-Al-Mn alloy by the addition of Ni. This enhancement may be related to the increase in the volume fraction of the α (fcc) phase at 873 K resulting from the addition of Ni.
2. The orientation dependence of the SM and SE strains accompanying the β_1/β_1' transformation in the Cu-Al-Mn alloy were calculated using phenomenological theory. A maximum SE strain of 10.3 pct in the direction lying between [001] and [102] and a minimum SE strain of 2 pct in the [111] direction were predicted. This orientation dependence of the SE is similar to that observed in other Cu-based SMAs.
3. An SE strain of about 7 pct was obtained in the direction 45 deg from RD in the {112}⟨110⟩ textured sheet. This value of the SE is over 3 times greater than the maximum value obtainable in other polycrystalline Cu-based SMAs.

ACKNOWLEDGMENTS

The authors thank Dr. L. Chandrasekaran, DERA (Farnborough, United Kingdom) for useful comments and for help in the preparation of the manuscript for publication. This work was supported by a Grant-in-Aid for Scientific Research and Development from the Ministry of Education, Science, Sports and Culture of Japan.

REFERENCES

1. T. Tadaki: in *Shape Memory Materials*, K. Otsuka and C.M. Wayman, eds., Cambridge University Press, Cambridge, United Kingdom, 1998, pp. 97-116.
2. J. Van Humbeeck and L. Delaey: in *The Martensitic Transformation in Science and Technology*, E. Hornbogen and N. Jost, eds., Butterworth-Heinemann, London, 1990, pp. 15-25.
3. S. Miyazaki and K. Otsuka: *Iron Steel Inst. Jpn. Int.*, 1989, vol. 29, pp. 353-76.
4. R. Kainuma, N. Satoh, X.J. Liu, I. Ohnuma, and K. Ishida: *J. Alloys Compounds*, 1998, vol. 266, pp. 191-200.
5. R. Kainuma, S. Takahashi, and K. Ishida: *Metall. Mater. Trans. A*, 1996, vol. 27A, pp. 2187-95.
6. R. Kainuma, S. Takahashi, and K. Ishida: *J. Phys. IV*, 1995, vol. 5 (C8), pp. 961-66.
7. Y. Sutou, R. Kainuma, and K. Ishida: *Mater. Sci. Eng. A*, 1999, vols. A273-A275, pp. 375-79.
8. Y. Sutou: Ph.D. Thesis, Tohoku University, Sendai, Japan, 2001.
9. S. Eucken and J. Hhirsch: *Mater. Sci. Forum*, 1990, vols. 56–58, pp. 487-92.

10. D.Y. Li, X.F. Wu, and T. Ko: *Acta Mater.*, 1990, vol. 38, pp. 19-24.
11. H. Inoue, N. Miwa, and N. Inakazu: *Acta Mater.*, 1996, vol. 44, pp. 4825-34.
12. L. Zhao, P.F. Willemse, J.H. Mulder, J. Beyer, and W. Wei: *Scripta Mater.*, 1998, vol. 39, pp. 1317-23.
13. Y.C. Shu and K. Bhattacharya: *Acta Mater.*, 1998, vol. 46, pp. 5457-73.
14. W. Chaoqun: *Proc. Int. Symp. on Shape Memory Materials on Shape Memory Materials '94*, C. Youyi and T. Hailing, eds., International Academic Publishers, Beijing, 1994, pp. 388-92.
15. P. Donner and S. Eucken: *Mater. Sci. Forum*, 1990, vols. 56–58, pp. 723-28.
16. B.L. Adams, S.I. Wright, and K. Kunze: *Metall. Trans. A*, 1993, vol. 24A, pp. 819-31.
17. X.J. Liu: Ph.D. Thesis, Tohoku University, Sendai, Japan, 1998.
18. M.S. Wechsler, D.S. Lieberman, and T.A. Read: *Trans. AIME*, 1953, vol. 197, pp. 1503-15.
19. J.S. Bowles and J.K. Mackenzie: *Acta Metall.*, 1954, vol. 2, pp. 129-37.
20. K. Otsuka, C.M. Wayman, K. Nakai, H. Sakamoto, and K. Shimizu: *Acta Metall.*, 1976, vol. 24, pp. 207-26.
21. T. Saburi and S. Nenno: *Proc. Int. Conf. on Solid-Solid Phase Transformations*, H.I. Aaronson, D.E. Laughlin, R.E. Sekerka, and C.M. Wayman, eds., AIME, New York, NY, 1982, pp. 1455-79.
22. H. Horikawa, S. Ichinose, S. Morii, S. Miyazaki, and K. Otsuka: *Metall. Trans. A*, 1988, vol. 19A, pp. 915-23.
23. H. Kato, T. Ozu, S. Hashimoto, and S. Miura: *Mater. Sci. Eng. A*, 1999, vol. A264, pp. 245-53.
24. N. Ono, A. Sato, and H. Ohta: *Mater. Trans. JIM*, 1989, vol. 30, pp. 756-64.
25. I. Dvorak and E.B. Hawbolt: *Metall. Trans. A*, 1976, vol. 6A, pp. 95-99.
26. Y. Sutou, T. Omori, J.J. Wang, R. Kainuma, and K. Ishida: Tohoku University Sendai, unpublished research, 2002.
27. Y. Suzuki: in *Shape Memory Materials*, K. Otsuka and C. M. Wayman, eds., Cambridge University Press, Cambridge, United Kingdom, 1998, pp. 133-48.